Journal of Alloys and Compounds 509 (2011) 172–176

Contents lists available at ScienceDirect

Journal of Alloys and Compounds

journal homepage: www.elsevier.com/locate/jallcom

In situ diffraction study of thermal decomposition in Maxthal Ti_2AlC

W.K. Pang[a], I.M. Low[a,*], B.H. O'Connor[a], V.K. Peterson[b], A.J. Studer[b], J.P. Palmquist[c]

[a] *Centre for Materials Research, Curtin University of Technology, GPO Box U1987, Perth, WA 6845, Australia*
[b] *The Bragg Institute, ANSTO, Locked Bag 2001, Kirrawee DC, NSW 2232, Australia*
[c] *Kanthal AB, Heating Systems R&D, P.O. Box 502, SE-734 27 Hallstahammar, Sweden*

ARTICLE INFO

Article history:
Received 11 April 2010
Received in revised form 31 August 2010
Accepted 1 September 2010
Available online 21 September 2010

Keywords:
Ceramics
Phase transitions
Neutron diffraction
Synchrotron radiation

ABSTRACT

The thermal stability of Ti_2AlC at elevated temperature (1000–1550 °C) in vacuum has been investigated using *in situ* neutron diffraction. At temperatures above 1400 °C, Ti_2AlC became unstable and began to decompose via sublimation of Al, resulting in a porous surface layer of TiC_x being formed. The apparent activation energy for Ti_2AlC decomposition was determined to be 85.7 ± 2.6 kJ mol^{-1}. The kinetics of isothermal phase decomposition was modelled using least-squares linear regression fitting and the Avrami equation. The corresponding least-squares regression exponent (R^2) and Avrami constants (k and n) for isothermal decomposition were determined to be 0.89, 0.268 min^{-n} and 0.1, respectively.

© 2010 Elsevier B.V. All rights reserved.

1. Introduction

MAX phases are nano-layered ceramics with the general formula $M_{n+1}AX_n$ (n = 1–3), where M is an early transition metal, A is a group-A element, and X is either carbon and/or nitrogen. These materials exhibit a unique combination of ceramic and metallics character [1–8]. They have a layered structure consisting of strong M–X bonds and relatively weak M–A bonds along the c-direction [8,9]. The unique combination of these interesting properties enables these ceramics to be promising candidate materials for use in diverse fields, especially in high temperature applications.

Diverse methods have been developed in recent years to increase the purity of Ti_2AlC samples. For instance, Kulkarni and Wu [10] reported the spark plasma sintering of Ti_2AlC using TiAl and carbon nanotubes powder mixture. In another study, Liang et al. [11] investigated the effect of additives on the purity of laser-induced self-propagating high-temperature synthesized Ti_2AlC using 2Ti/Al/C powders as starting materials. The use of Sn additive was shown to improve the phase purity Ti_2AlC.

Hitherto, there is very little information on the high-temperature thermal stability of MAX phases in vacuum, and the process of phase decomposition is also poorly understood. It is generally accepted that MAX phases do not melt congruently, but decompose into binary carbide/nitride *via* excluding the A elements, and the decomposition temperature is environment-dependent [12].

Based on first-principles calculations, Wang et al. [8] proposed that the thermal dissociation of Ti_2AlC may involve the outward diffusion of Al. In terms of its electronic structure, Du et al. [9] reported that Ti_2AlC is less stable than Ti_2SC. Qin et al. [13,14] studied the phase stability of Ti_2AlC at high temperature (800–1300 °C) and high hydrostatic pressure (3.0–5.0 GPa). They reported that the decomposition temperature of Ti_2AlC into AlTi and TiC was pressure-dependent. For instance, at 4.0 GPa, decomposition of Ti_2AlC was detected at 1030 °C and at 890 °C when the pressure was increased to 5.0 GPa. However, the kinetics of Ti_2AlC thermal decomposition in vacuum is still poorly understood. In another study, Zhou et al. [15] observed the transformation of Ti_2AlC into Ti_3AlC_2 during hot-pressing and the subsequent decomposition of Ti_3AlC_2 into TiC_x *via* the depletion of Al. Similar processes (i.e. from lower order, e.g. n = 1, to higher order, e.g. n = 2, 3) were observed by Hu et al. [16,17] for the decomposition of Ta_2AlC into Ta_4AlC_3 and Nb_2AlC to Nb_4AlC_3 in Argon atmosphere at elevated temperatures, probably through intercalation of the formed binary carbide (e.g. TaC) into the 211 structure (e.g. Ta_2AlC).

This paper describes the use of *in situ* neutron diffraction to characterize the thermal dissociation of Ti_2AlC in high vacuum at temperatures up to 1550 °C. The activation energy for the decomposition of Ti_2AlC was determined using Arrhenius equation. The kinetics of phase decomposition was modelled using the Avrami equation and the Avrami constants were evaluated. The characteristics of thermal stability and phase transitions in Ti_2AlC are discussed.

* Corresponding author. Tel.: +61 8 9266 7544/437 023 397; fax: +61 8 9266 7544.
E-mail address: j.low@curtin.edu.au (I.M. Low).

0925-8388/$ – see front matter © 2010 Elsevier B.V. All rights reserved.
doi:10.1016/j.jallcom.2010.09.019

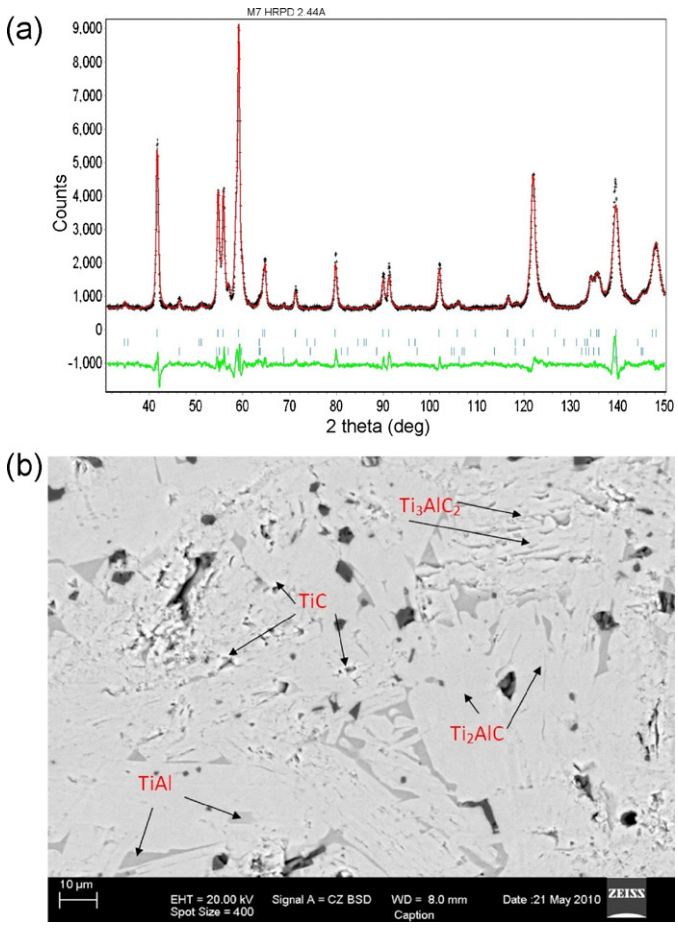

Fig. 1. (a) Rietveld refinement using high-resolution powder neutron diffraction data (λ = 2.439 Å), and (b) back-scattered electron micrograph of as-sintered Ti_2AlC showing the existence of TiC, Ti_3AlC_2 and TiAl impurity phases. The dark regions in the micrograph are due to voids or grain pull-outs during sample polishing.

2. Experimental details

Maxthal Ti_2AlC samples (15 mm in diameter and 50 mm in length) were fabricated using a proprietary method developed by Kanthal AB, Sweden. The density of these samples was determined to be $4.03 \pm 0.03\,g/cm^3$ with ~1% porosity. High-resolution neutron powder diffraction (HRPD) was used to characterize the as-prepared Ti_2AlC and indicate the sample contained 5.1 wt% TiC, 4.1 wt% TiAl and 6.5 wt% Ti_3AlC_2 as impurities (Fig. 1a). These relatively minor amounts of impurity phases are expected to have an insignificant effect on the kinetics of Ti_2AlC decomposition. Fig. 1b shows the corresponding microstructure of the as-sintered sample where the existence of TiC, Ti_3AlC_2 and TiAl impurity phases is evident.

High temperature *in situ* neutron diffraction data were collected using Wombat, the high intensity neutron powder diffractometer at the OPAL research reactor at ANSTO in Australia [18]. Data were collected using a neutron beam with a wavelength of 1.660 Å and an incident beam height of 20 mm. The wavelength was determined using an external standard α-Al_2O_3 (NIST Standard Reference Material 676). Diffraction patterns were collected using a 2D area detector with a 2θ range of 15–135° with a step size of 0.125°. An oscillating radial collimator with a 1 min period was located in front of the detector to eliminate stray diffraction from the furnace.

Rietica 1.7.7 [19] was used for phase identification and Rietveld refinement. The optimized parameters during refinement were background coefficients, zero-shift error, peak shape parameters, cell parameters, and anisotropic thermal factors. The residual plots for the refinement and the refinement figures of merit (the phase Bragg *R*-factors (R_B), the pattern weighted *R*-factor (R_{wp}), the expected *R*-factor (R_{exp}), and the goodness-of-fit (χ^2)), were used to assess refinement quality. In Rietica, χ^2 is defined as the square of the ratio of R_{wp} to R_{exp}.

Solid cylindrical bars with dimensions 15 mm (diameter) × 20 mm (height), which had been cut from the as-received sample of Ti_2AlC, were used in this study. The temperature of the sample environment was controlled by a closed cylindrical niobium vacuum furnace (10^{-6} to 10^{-8} torr). The sample was held by a vanadium wire and heated to 1000 °C at a heating rate of 10 °C/min and thereafter at 5 °C/min to 1550 °C. The dwell times between 1000 and 1550 °C are shown in Table 1. Diffraction patterns were collected every minute during the experiment.

Table 1
Heating schedule during the *in situ* neutron diffraction study.

Temperature (°C)	Dwell time (min)	Temperature (°C)	Dwell time (min)
1000	30	1400	200
1100	30	1450	200
1200	30	1500	200
1300	30	1550	200

The decomposition rates (k) at different temperatures were calculated and the corresponding apparent activation energies (E) were determined using the Arrhenius' equation,

$$k = k_0 \exp\left(-\frac{E}{RT}\right) \quad (1)$$

where k_0 is constant, R is the gas constant ($8.3145\,J\,K^{-1}\,mol^{-1}$) and T is absolute temperature [20].

The kinetics of isothermal decomposition of Ti_2AlC at 1550 °C was modelled using the Avrami equation to depict the fraction of decomposed Ti_2AlC (y) as a function of time:

$$y = \exp(-kt^n) \quad (2)$$

where k and n are the Avrami rate constant and Avrami exponent, respectively [21].

Grazing-incidence synchrotron radiation diffraction (GISRD) was used to understand the depth-dependent sample composition of vacuum-decomposed Ti_2AlC. In GISRD, the intensity-weighted penetration depth (d) of X-ray penetration into the sample depends on the value of incidence angle (α) and the energy of the X-ray beam (E). The penetration depth is described by:

$$d = \frac{2\alpha}{\mu} \quad (3)$$

where μ is the linear attenuation coefficient of the material [22]. SRD depth profiles of vacuum-decomposed Ti_2AlC were measured at the Photon Factory using the BIGDIFF on beamline 20B [23]. Image-plates were used to record the diffraction patterns at a fixed wavelength of 0.7 Å and incidence angles of 0.1°, 0.4°, 0.6°, 0.8°, 1.0°, and 3.0°. A thin slice was cut from the decomposed Ti_2AlC sample after cooling from 1550 °C and used for GISRD to depth profile the near-surface phase composition. The surface microstructure of the decomposed Ti_2AlC was examined by scanning electron microscopy using a Zeiss EVO 40XVP.

3. Results and discussion

The Rietveld method was used to analyze the neutron diffraction patterns. The residual values for the refinements R_{wp} and R_{exp} ranged from 3.40 to 3.67 and 2.45 to 2.65, respectively. The goodness-of-fit, χ^2, ranged from 1.90 to 2.43. The good quality of fits (Fig. 2) indicates that the quality of the refinements was acceptable. Based on the refinements, the phase transformation of Maxthal-Ti_2AlC at elevated temperatures, as revealed by *in situ* neutron diffraction, is shown in Fig. 3. At temperatures above 1300 °C, the impurities TiAl and Ti_3AlC_2 decomposed completely after annealing at 1300 °C for 30 min. The latter is believed to decompose to TiC_x *via* sublimation of Al (Eq. (4a)). In contrast, TiAl decomposes through sublimation of the Al and possibly Ti elements (see Eq. (4b)) by virtue of their high vapour pressures [24].

$$Ti_3AlC_2 \rightarrow 3TiC_{0.67} + Al \quad (4a)$$

$$TiAl \rightarrow Ti + Al \quad (4b)$$

At higher temperatures, Ti_2AlC decomposes to TiC_x, with the concomitant sublimation of Al (Eq. (5)). The vapour pressure of Al rises rapidly from $\sim 7 \times 10^{-3}$ torr at 1200 °C to ~0.5 torr at 1500 °C, whereas the vapour pressure for Ti is 3 orders of magnitude lower at this temperature [24]. We hypothesize that Al becomes volatile and sublimes continuously in high vacuum, leading to severe decomposition of Ti_2AlC with the concomitant formation of non-stoichiometric TiC_x on the surface, i.e.

$$Ti_2AlC \rightarrow 2TiC_{0.5} + Al \quad (5)$$

This observation is consistent with the theoretical work of Wang et al. [8], although non-stoichiometric Ti_2Al_xC was not detected in

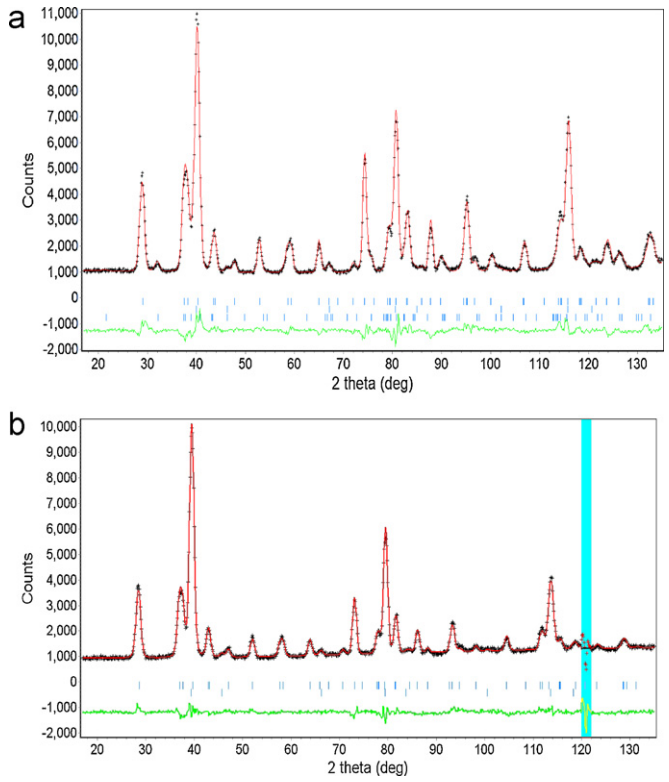

Fig. 2. The Rietveld profile fit of diffraction data of Ti_2AlC collected at (a) room temperature ($\chi^2 = 2.1$, $R_{wp} = 4.1$, $R_{exp} = 2.3$, $R_B = 0.9–2.0$) before decomposition and (b) 1550 °C after decomposition ($\chi^2 = 2.6$, $R_{wp} = 4.1$, $R_{exp} = 2.5$, $R_B = 1.2–2.2$). Measured patterns indicated by black crosses, calculated pattern indicated by red solid line. Intensity differences between the two patterns are shown as green line along the bottom of the plot. Vertical bars represent the allowable peak position of each of the phases [top: Ti_2AlC (ICSD #157767), middle: TiC (ICSD #1546), and bottom: Ti_3AlC_2 (ICSD #153226)]. (For interpretation of the references to color in this figure legend, the reader is referred to the web version of this article.)

this work. The results of this work are different from those of Kisi et al. [25] who reported that the partial depletion of Al from Ti_2AlC and its subsequent intercalation with TiC led to the formation of Ti_3AlC_2. In contrast, we propose here the full depletion of Al during the decomposition of Ti_2AlC or Ti_3AlC_2 with the concomitant formation of TiC_x as described by Eqs. (4) and (5). The discrepancy between the findings of this study and the work of Kisi et al. may be attributed to the dynamic high vacuum of this study compared with the flowing argon environment studied by Kisi et al. Under flowing argon, the pressure in the furnace environment is higher

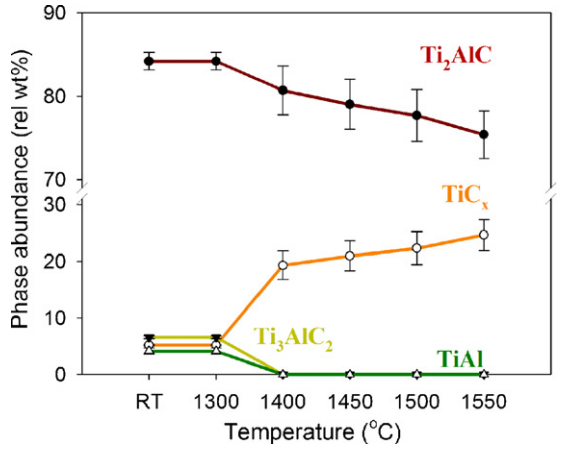

Fig. 3. Phase decomposition of Ti_2AlC during vacuum-annealing up to 1550 °C.

than the vapour pressure of Al, resulting in restricted release of Al. In contrast, the pressure of the furnace environment used in this study remained fairly constant at 10^{-6} to 10^{-8} torr during annealing, which is significantly higher than the vapour pressure of Al. As a result, Al will sublime readily by virtue of its high vapour pressure, causing decomposition of Ti_2AlC.

This hypothesis is further supported by the observation of a grey or silver coating on the sample and furnace inserts after decomposition, the sample being black before decomposition. The decomposition rates at 1450, 1500, and 1550 °C were calculated by examining phase abundances as a function of dwell time at these temperatures (see Fig. 4). Applying the reaction rates obtained from

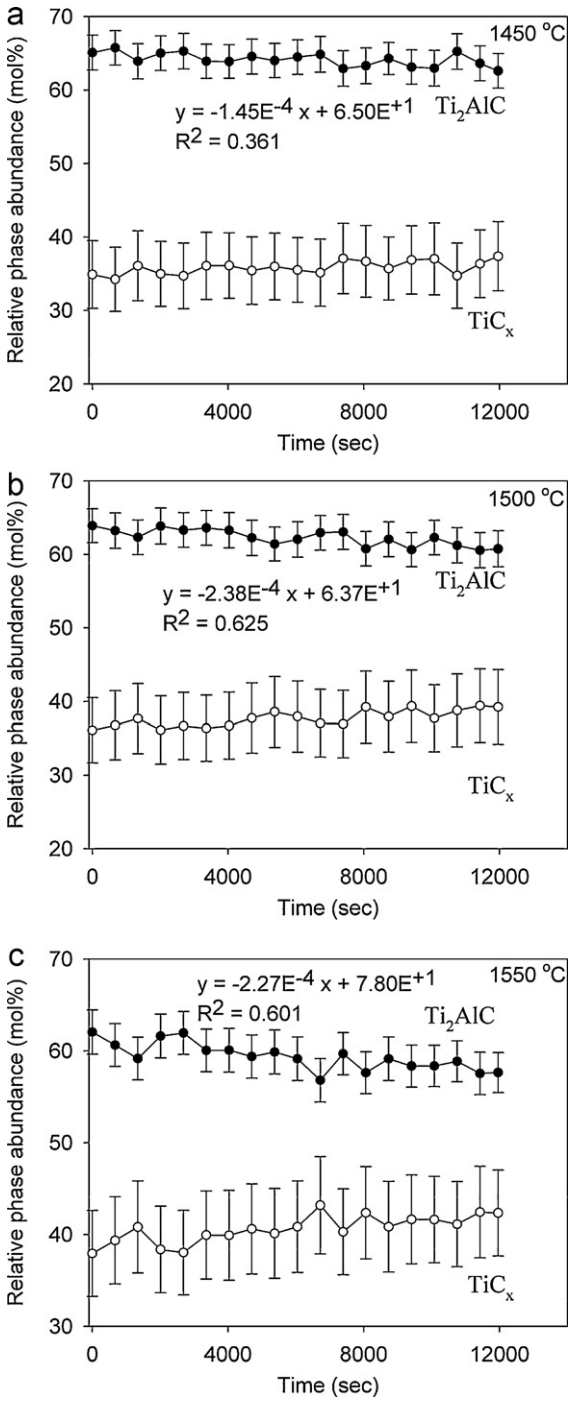

Fig. 4. Phase abundances versus soaking times for isothermal dissociation of Ti_2AlC at (a) 1450 °C, (b) 1500 °C, and (c) 1550 °C.

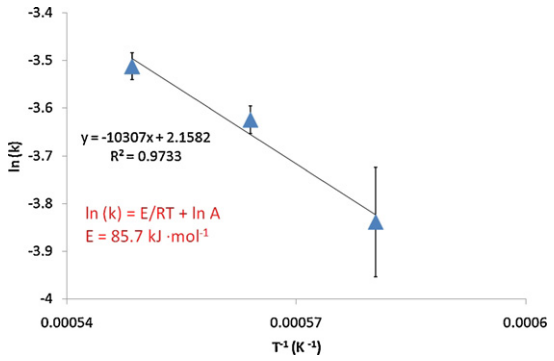

Fig. 5. Regression line with negative slope for decomposition of Ti_2AlC showing that the activation energy was determined to be 85.7 ± 2.6 kJ/mol.

the refinement to the Arrhenius equation, the Arrhenius plot (see Fig. 5) shows a linear line with a negative slope. The apparent activation energy of Ti_2AlC decomposition in vacuum was determined to be 85.7 ± 2.6 kJ mol^{-1}.

The kinetics of phase decomposition of Ti_2AlC during vacuum-annealing at elevated temperature was modelled using both the least-squares linear regression and the Avrami equation (see Fig. 6). The corresponding least-squares regression exponent (R^2) and Avrami constants (k and n) of isothermal decomposition were determined to be 0.89, 0.268 min^{-n} and 0.1, respectively. This suggests that the kinetics of Ti_2AlC decomposition is better described by a linear rate reaction rather than an exponential Avrami rate reaction. Nevertheless, the latter rate reaction cannot be ruled out. Assuming both rate reactions were involved in the decomposition kinetics, this implies that the decomposition process is driven by the highly restricted outward diffusion of Al from the bulk to the surface of the sample, since the obtained value of n is much smaller than 1.0.

When the vapour pressure of Al exceeds the ambient pressure in the vacuum furnace, bubbles form which eventually appear as voids on the near-surface of decomposed Ti_2AlC, as clearly shown by the SEM images in Fig. 7.

Near-surface compositions of decomposed Ti_2AlC were also depth profiled using grazing-incidence synchrotron radiation (see Fig. 8). Since the mass attenuation coefficient and density of TiC are 22.0 cm^2/g [26] and 4.92 g/cm^3, respectively, the corresponding penetration depths for the synchrotron radiation beam can be calculated from Eq. (3) as shown in Table 2. Based on the GISRD results, a layer of TiC_x with a thickness of at least 10-μm can be deduced to have formed on the surface of decomposed

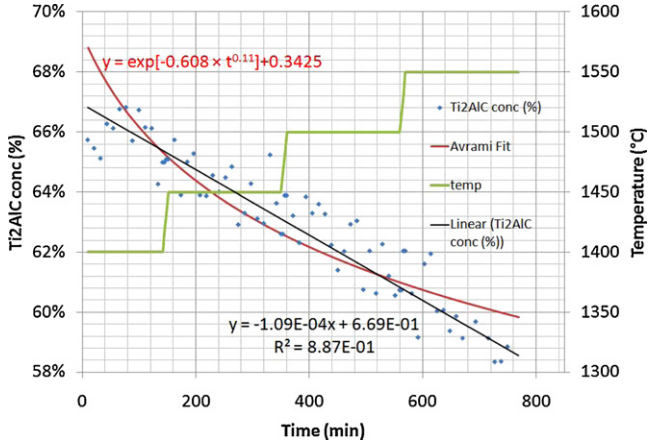

Fig. 6. Least-squares linear regression and Avrami fits of phase decomposition in vacuum-annealed Ti_2AlC at elevated temperature from 1300 to 1500 °C.

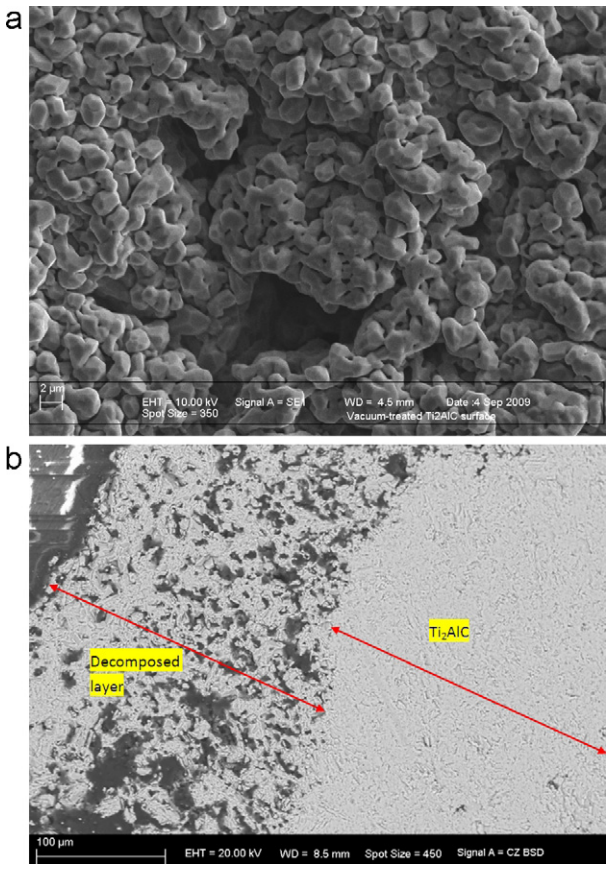

Fig. 7. SEM micrograph showing (a) the porous surface microstructure and (b) the cross-sectional microstructure of Ti_2AlC decomposed at 1550 °C for 200 min.

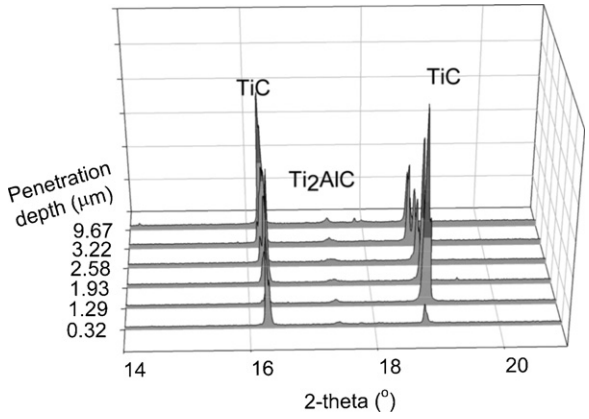

Fig. 8. Grazing-incidence diffraction plots showing the composition depth profiles of Ti_2AlC decomposed at 1550 °C for 200 min.

Table 2
The relation between grazing-incident angles and their corresponding penetration depths.

Incident angle (degree)	Depth (μm)
0.10	0.32
0.40	1.29
0.60	1.93
0.80	2.58
1.00	3.22
3.00	9.67

Ti_2AlC. The slight depth-dependent variations of TiC_x and Ti_2AlC peak intensities suggest the existence of a very modest phase composition gradation within the near-surface layer of decomposed Ti_2AlC at 1550 °C in vacuum. A similar but much more pronounced phase composition gradation has also been observed within the decomposed TiC_x surface layer in vacuum-annealed Ti_3SiC_2 [27,28].

The existence of a pronounced composition gradation in this system is not as obvious as in vacuum-annealed Ti_3SiC_2 that we previously observed [22,23]. This discrepancy may be attributed to two factors. First, the formation of a relatively thick (~200 μm) decomposed TiC_x layer in vacuum-annealed Ti_2AlC (see Fig. 7b) when compared to less than 50 μm in vacuum-annealed Ti_3SiC_2 [23]. Second, the energy of the synchrotron radiation used in this study was insufficient to penetrate to a depth greater than 200 μm which would be required to map the complete composition gradation at the interface between TiC_x and the Ti_2AlC substrate. In this study, a maximum depth of only ~10 μm was probed which lay completely within the homogeneous decomposed TiC_x layer. Photons of much higher energy would be required to map the composition gradation over a depth of ~200 μm for the vacuum-annealed Ti_2AlC.

4. Conclusions

The high-temperature thermal stability of Ti_2AlC in a high vacuum has been studied using *in situ* neutron diffraction. Ti_2AlC was susceptible to decomposition at temperatures above 1400 °C through sublimation of high vapour pressure Al, resulting in a porous surface layer of TiC_x being formed. The apparent activation energy for Ti_2AlC decomposition in high vacuum was determined to be $85.7 \pm 2.6\ kJ\ mol^{-1}$. The kinetics of isothermal phase decomposition was modelled using least-squares linear regression and the Avrami equation. The corresponding linear regression exponent (R^2) and Avrami constants (k and n) of isothermal decomposition were determined to be 0.89, $0.268\ min^{-n}$ and 0.1, respectively, with the latter being indicative of highly restricted diffusion of Al between the octahedral channels of TiC_x. Composition depth-profiling using grazing-incidence synchrotron radiation diffraction has revealed the existence of a very modest phase composition gradation within the first 10 μm of the 200 μm thick TiC_x layer of decomposed Ti_2AlC.

Acknowledgements

This work is part of a broader project on the thermal stability of ternary carbides which is funded by an ARC Discovery-Project grant (DP0664586) and an ARC Linkage-International grant (LX0774743) for one of us (IML). Neutron powder diffraction data were collected at the OPAL Research Reactor at ANSTO, with financial support from AINSE (08/329) and the Bragg Institute (MI1488). Synchrotron radiation diffraction data were collected at the Australian National Beamline Facility at the Photon Factory in Japan, operated by the Australian Synchrotron, Victoria, Australia with financial support from the Australian Synchrotron (P1334). We thank Dr. G. Foran and Dr. B. Johannessen of the Australian National Beamline Facility for experimental assistance in the collection of synchrotron data.

References

[1] M.W. Barsoum, Prog. Solid State Chem. 28 (2000) 201.
[2] J.Y. Wang, Y.C. Zhou, Annu. Rev. Mater. Res. 39 (2009) 415.
[3] Z.M. Sun, Inter. Mater. Rev., in press.
[4] B.H. Zhang, Y.W. Bao, Y.C. Zhou, J. Mater. Sci. Technol. 25 (2009) 1.
[5] M.W. Barsoum, T. El-Raghy, Am. Sci. 89 (2001) 334.
[6] Z.J. Lin, M.S. Li, J.Y. Wang, Y.C. Zhou, Scripta Mater. 58 (2008) 29.
[7] X.H. Wang, Y.C. Zhou, Oxid. Met. 59 (2003) 303.
[8] J. Wang, Y.C. Zhou, T. Liao, J. Zhang, Z. Lin, Scripta Mater. 58 (2008) 227.
[9] Y.L. Du, Z.M. Sun, H. Hashimoto, Phys. Rev. B 405 (2010) 720.
[10] S.R. Kulkarni, A.V. Wu, J. Alloys Compd. 490 (2010) 155.
[11] B. Liang, M. Wang, X. Li, S. Sun, Q. Zou, Y. Mu, X. Li, J. Alloys Compd. 501 (2010) L1.
[12] P. Eklund, M. Beckers, U. Jansson, H. Hogberg, L. Hultman, Thin Solid Films 518 (2010) 1851.
[13] J. Qin, D. He, C. Chen, J. Wang, J. Hu, B. Yang, J. Alloys Compd. 462 (2008) L24.
[14] J. Qin, D. He, L. Lei, P. An, L. Fang, Y. Li, F. Wang, Z. Kou, J. Alloys Compd. 476 (2009) L8.
[15] A. Zhou, C. Wang, Y. Huang, Mater. Sci. Eng. A A352 (2003) 333.
[16] C. Hu, J. Zhang, Y. Bao, J. Wang, M. Li, Y. Zhou, Z. Metallkd. 99 (2008) 8.
[17] C. Hu, F. Li, J. Zhang, J.M. Wang, J.Y. Wang, Y. Zhou, Scripta Mater. 57 (2007) 893.
[18] A.J. Studer, M.E. Hagen, T.J. Noakes, Physica B 385–386 (2006) 1013.
[19] www.rietica.org.
[20] A.K. Galwey, M.E. Brown, Thermochim. Acta 386 (2002) 91.
[21] J.W. Cahn, Acta Metall. 4 (1956) 572.
[22] G. Lim, W. Parrish, C. Ortiz, M. Belloto, M. Hart, J. Mater. Res. 2 (1987) 471.
[23] B. O'Connor, A. van Riessen, J. Carter, G.R. Burton, R.F. Garrett, D.J. Cookson, J. Am. Ceram. Soc. 80 (1997) 1373.
[24] www.veeco.com/library/Learning_Center/Growth_Information/Vapor_Pressure_Data_For_Selected_Elements/index.aspx.
[25] E.H. Kisi, E. Wu, J.S. Zobec, et al., J. Am. Ceram. Soc. 90 (2007) 1912.
[26] http://physics.nist.gov/cgi-bin/Xcom/xcom3_2.
[27] I.M. Low, Mater. Lett. 58 (2004) 927.
[28] I.M. Low, Z. Oo, K.E. Prince, J. Am. Ceram. Soc. 90 (2007) 2610.